Effects of transhydrogenase and growth substrates on lipid D/H ratios in *Desulfovibrio alaskensis* G20

William D. Leavitt[1,2*], Theodore M. Flynn[3], Melanie K. Suess[1], Alexander S. Bradley[1,4*]

1. Department of Earth and Planetary Sciences, Washington University in St. Louis, Saint Louis, MO, USA

2. Department of Earth Sciences, Dartmouth College, Hanover, NH, USA

3. Biosciences Division, Argonne National Laboratory, Argonne, IL, USA

4. Division of Biology and Biomedical Sciences, Washington University in St. Louis, Saint Louis MO, USA

***Correspondence**: William D. Leavitt, Department of Earth and Planetary Sciences, Washington University in St. Louis, 1 Brookings Drive, Saint Louis, MO 63130 USA
wleavitt@eps.wustl.edu

***Correspondence**: Alexander S. Bradley, Department of Earth and Planetary Sciences, Washington University in St. Louis, 1 Brookings Drive, Saint Louis, MO 63130 USA
abradley@eps.wustl.edu

Keywords: lipid hydrogen isotopes, electron bifurcation/confurcation, biomarkers, dissimilatory sulfate reduction.

Abstract

Microbial fatty acids preserve metabolic and environmental information in their ratios of deuterium (D) to hydrogen (H). This ratio is influenced by parameters that include the D/H of water in the microbial growth environment, and biosynthetic fractionations between water and lipid. In some microbes, this biosynthetic fractionation has been shown to vary systematically with central energy metabolism, and controls on fatty acid D/H may be linked to the intracellular production of NADPH. We examined the apparent fractionation between media water and the fatty acids produced by *Desulfovibrio alaskensis* G20. Growth was in batch culture with malate as an electron donor for sulfate respiration, and with pyruvate and fumarate as substrates for fermentation or sulfate respiration. A larger fractionation was observed as a consequence of respiratory or fermentative growth on pyruvate than growth on fumarate or malate. This difference correlates with opposite flows of electrons through the electron bifurcating/confurcating transhydrogenase NfnAB. When grown on malate or fumarate, mutant strains of *D. alaskensis* G20 containing transposon disruptions in a *nfnAB* paralog show different fractionations than the wild type strain. This isotopic phenotype is muted during fermentative growth on pyruvate, and it is absent when pyruvate is a substrate for sulfate reduction. All strains and conditions produced similar fatty acid profiles, and the D/H of individual lipids changed in concert with the mass-weighted average. We found that fractionation correlated strongly with growth rate, a pattern that has also been observed in the fractionation of sulfur isotopes during dissimilatory sulfate reduction by sulfate reducing bacteria.

1 Introduction

The structures and isotopic compositions of lipids preserve information about organisms that can be archived in sediments and rocks over geological time scales. Understanding how to interpret this information is a central task of organic geochemistry. Lipid structures can be affiliated to particular groups of organisms (Pearson, 2014), and ratios of carbon isotopes in lipids record information about carbon sources and assimilation pathways (Hayes, 2001). The ratio of deuterium to hydrogen (D/H) in lipids derived from environmental samples has been observed to relate to the D/H in environmental water (Hayes, 2001; Sauer et al., 2001). More recently, it was shown in a range of aerobic microorganisms that the fractionation of hydrogen isotopes between media water and lipids varied with changes in growth substrate (Zhang et al., 2009). Experiments with anaerobes have shown less systematic changes in lipid D/H as a function of energy metabolism, although strong differences have been observed between pure cultures and co-cultures of the same organisms (Dawson et al., 2015; Osburn, 2013).

Observations that lipid D/H varies as a function of growth substrate in many microorganisms raises the question of what specific metabolic mechanisms are responsible. Zhang et al. (2009) considered several explanations, and through a process of elimination, deduced that observed differences in lipid D/H must be a consequence of differences in the NAD(P)H that serves as a hydride donor during lipid biosynthesis. These authors pointed out that cells have multiple pathways for producing NAD(P)H, and that the relative importance of each of these mechanisms varies with differences in growth conditions. One mechanism considered was alteration of the D/H ratio of the transferrable hydride in NAD(P)H by transhydrogenase enzymes. This suggestion stems from two key observations. First, up to half of the hydrogen atoms in microbial lipids are derived directly from NADPH during biosynthesis (Jackson, 2003; Saito et al., 1980). Second, in vitro observations of the hydrogen isotope fractionation imparted by transhydrogenase suggest that it is very large (> 800‰) (Bizouarn et al., 1995; Jackson et al., 1999; Venning et al., 1998).

In this study, we vary substrates and use mutant strains to investigate the importance of a transhydrogenase (NADH-dependent reduced ferredoxin:NADP oxidoreductase; NfnAB) on the lipid D/H ratios in an anaerobic microorganism, *Desulfovibrio alaskensis* G20. Recent work has suggested that NfnAB plays an important role in energy conservation in this microbe (Price et al., 2014). The role of NfnAB varies as a function of the growth substrate. During growth on malate, for example, NfnAB is predicted to catalyze an electron bifurcation, in which NADPH reduces ferredoxin as well as NAD^+, with NADH as a product (Figure 1). Conversely, during growth on pyruvate, NfnAB is predicted to catalyze electron confurcation and the production of NADPH from NADH, $NADP^+$, and reduced ferredoxin. Since the transhydrogenase reaction catalyzed by NfnAB is predicted to be in opposite directions during growth on pyruvate versus that on malate, the lipids produced under each condition should have different D/H ratios if NfnAB is indeed a significant source of isotope fractionation for intracellular hydrogen. Furthermore, the role of NfnAB in hydrogen isotope fractionation can be further explored using mutant strains of *D. alaskensis* G20 in which the NfnAB-2 loci have been disrupted.

2 Material and Methods

2.1 Strains, growth media, culture conditions and biomass sampling

Wild type *Desulfovibrio alaskensis* G20 was obtained along with two mutant strains from the library collection at Lawrence Berkeley National Laboratory. Each mutant contains a Tn5 transposon insertion into a gene of interest. These insertions (Kuehl et al., 2014) were into the genes *nfnA*-2 at locus Dde_1250 (strain JK00256) and *nfn*B-2 at locus Dde_1251 (JK01775). Hereafter, these strains are referred to as the *nfnA*-2 and *nfnB*-2 mutants. These loci encode the subunits for one of two paralogs of NfnAB in *D. alaskensis* G20.

All strains were resuscitated from 10% glycerol freezer stocks stored at -80 °C. Resuscitated strains were inoculated into serum bottles containing approximately 50 ml of a rich lactate/sulfate medium containing yeast extract (MOY_LS) and incubated at 30 °C. After reaching stationary phase, strains were then serially transferred three times in a defined lactate/sulfate (80 mM/40 mM) medium (MO_LS). Late-log phase cultures of the third transfer were diluted 1 to 100 into duplicate bottles for each isotope fractionation experiment. There were five experimental growth conditions, which combined an electron donor and 40 mM sulfate (for sulfate respiration), or an electron donor alone for fermentation. The five conditions were: pyruvate/sulfate respiration, malate/sulfate respiration, fumarate/sulfate respiration, pyruvate fermentation, fumarate fermentation.

The basal growth medium recipe (MO) is as follows: 8 mM magnesium chloride, 20 mM ammonium chloride, 0.6 mM calcium chloride, 6 mL/L trace elements solution (see below), 0.12 mM of $FeCl_2$ (125mM)+EDTA (250 mM) stock solution, 30 mM Tris-HCl (2M, pH 7.4 stock). Sodium thioglycolate (0.12 g/L) was added as a reductant following initial degassing. MO medium containing yeast extract (MOY) was generated by adding a final concentration of 0.1% yeast extract to MO medium from an anoxic sterile stock. Media were made anaerobic by degassing with O_2-free N_2 that had been filtered through sterile 0.22 μm syringe filters. Solutions were degassed for 2 hours per liter. The pH of the final medium was adjusted to 7.2 using sterile and anoxic HCl or NaOH, autoclave-sterilized, and then cooled under sterile O_2-free N_2. After cooling, phosphate solution was added to a final concentration of 2 mM from a sterile, anoxic stock solution of K_2HPO_4+NaH_2PO_4. Thauer's Vitamins were added from a 1000x stock (Rabus et al., 2015). The initial concentration of sulfate was always 40 mM (except in fermentation experiments) and was added directly to the medium from a sterile and anoxic stock solution of Na_2SO_4 solution. Electron donors (sodium lactate, sodium pyruvate, malic acid, or sodium fumarate) were prepared separately as 1M stocks in MilliQ water, adjusted to a pH of 7.2, and degassed in a manner similar to the basal media. These anoxic stocks were then added to the basal media using aseptic technique.

Growth rate was determined by monitoring changes in optical density (OD_{600}) over time for each experiment. Replicate cultures were tracked through log-phase and into early

stationary phase, at which point they were harvested for biomass. Growth rate was calculated using a modified logistic equation (Rabus et al., 2006) and averaged across the apparent log-phase of growth. For experiments showing clear diauxic growth we calculated an interval-weighted average growth rate to account for both phases.

Duplicate 50mL cultures were harvested at the onset of early stationary phase by opening the serum bottles, decanting the remainder of each serum bottle (> 40mL) into sterile 50mL conical tubes, and centrifuging at 5000 rpm at 5 °C for 30 minutes. Spent medium was decanted into a fresh 50mL tube and frozen at -80 °C for later analysis of the isotopic composition of water therein. The biomass pellet was frozen at -80 °C, transferred to a pre-combusted 4mL borosilicate glass vial, lyophilized, and weighed.

2.2 Fatty acid extraction and quantitation

Samples were simultaneously extracted and derivatized to fatty acid methyl ethers (FAMEs) by adding a mixture of hexane, methanol and acetyl chloride to the lyophilized cell pellet, followed by heating at 100 °C for 10 minutes, and extraction with hexane (Rodriguez-Ruiz et al., 1998; Zhang et al., 2009). This procedure was also concurrently performed on two isotope standards, myristic acid and phthalic acid, for which the δD of non-exchangeable hydrogen was known (Qi and Coplen, 2011). Each sample was reacted with acid-activated copper to remove reduced sulfur compounds, and then concentrated under a stream of dry hydrocarbon-free nitrogen.

Individual FAMEs were analyzed using a HP 7890 gas chromatograph fitted with a split/splitless injector operated in splitless mode, equipped with a J&W DB-5 fused silica capillary column (30 m length, 0.25-mm inner diameter, and 0.25-μm film thickness) and coupled to an Agilent 6973 mass selective detector. FAME identifications were based on mass spectra and retention times. Quantities were determined by peak area as calculated in Chemstation (Agilent Technologies, Santa Clara, CA) relative to a known amount of co-injected methyl tetracosanoate (C24:0) provided by Dr. A. Schimmelmann (Indiana University).

2.3 Isotopic measurements and data handling

Hydrogen-isotopic compositions of individual FAMEs were determined using a TraceGC gas chromatograph fitted with a column identical to that on the Agilent GC, and coupled to a Thermo Scientific Delta V Plus isotope-ratio-monitoring mass spectrometer via a Thermo GC-Isolink pyrolysis interface at 1400 °C. Column temperature was initially 60 °C and was increased at a rate of 6 °C min^{-1} until reaching a final temperature of 320 °C. Hydrogen isotope ratios of individual lipids were determined relative to coinjected methyl tetracosanoate (C24:0) of known isotopic composition, provided by Dr. Schimmelmann (Indiana University). Instrumental precision was regularly monitored by analyzing RMS error on mixtures of FAMEs and of *n*-alkanes of known isotopic composition, also purchased from Dr. Schimmelman (Indiana University). Over the measurement period the mean RMS error on a mixture of 8 FAMEs was 5.5‰ (n = 286). Samples were discarded if they were not bracketed by injections of FAMEs mixture with

an RMS better than 7‰. H_3 factors were determined daily and had a mean value of 2.98 ± 0.3 ppm/nA. All FAME isotopic compositions were corrected by mass balance for the hydrogen present in the methyl group, calculate from them myristic acid and phthalic acid isotopic standards. Samples were reinjected (pseudoreplicates) three to six times, and errors were propagated following established methods (Polissar and D'Andrea, 2014). Statistical analyses were performed in either Prism (GraphPad Software, Inc., La Jolla, CA) or R (RCoreTeam, 2015).

All D/H ratios are reported as δD values relative to V-SMOW, and fractionations are reported as apparent fractionations between media water and lipid by the equation

$$\varepsilon_{lipid} = 1000\left(\frac{1000 + \delta D_{lipid}}{1000 + \delta D_{water}} - 1\right)$$

The δD_{water} of growth media water was measured using a Picarro L2130-*i* cavity ring-down spectrometer at Northwestern University.

2.4 Comparative analysis of *nfnAB* sequences

We constructed a gene tree of *nfnAB* sequences by retrieving data from two public repositories of annotated genomes: the SEED database (Overbeek et al., 2014) and UniProt (The UniProt Consortium, 2014). Sequences that were homologous to *nfnAB* from *D. alaskensis* G20 were identified using an amino acid BLAST search. This approach identified 1,575 putative *nfnAB* sequences from sequenced genomes. For this study, this list was manually refined to include only known sulfate reducers, methanogens, and other anaerobes. The 104 retained *nfnAB* sequences were closely related to that of *D. alaskensis* G20 using established criteria (Marti-Renom et al., 2000), with > 40% amino acid identity and BLASTP percent identities ranging from 45–77%. *D. alaskensis* G20 has two copies of the nfnAB gene that share 85% amino acid identity. A multiple sequence alignment of the 104 *nfnAB* sequences was created using MUSCLE (Edgar, 2004) and checked manually using AliView (Larsson, 2014). Alignments in FASTA format are available to download in the Supplementary Materials. Pairwise distances for construction of a phylogenetic tree were calculated using the RAxML maximum likelihood algorithm (Stamatakis, 2006) with the program raxmlGUI (Silvestro and Michalak, 2012). The tree itself was generated using the Interactive Tree of Life software (Letunic and Bork, 2011).

3. Results

3.1 Growth rates

Growth experiments revealed distinct physiological and isotopic phenotypes among the wild type and mutant strains of *D. alaskensis* G20. Growth rates are reported in Table 1 and growth curves are plotted in Figure 2. Some conditions exhibited diauxic growth; we report the average growth rate through both phases.

Some growth conditions showed clear phenotypic differences between the *D. alaskensis* G20 wild type and the two *nfnAB-2* mutants. Each strain was able to grow as a sulfate reducer using malate as an electron donor, but the growth rate of the mutants was only 22% that of the wild type. Similarly, with fumarate as an electron donor coupled to sulfate reduction, mutant growth rate was roughly 10% that of the wild type. A repression in growth rate (22% of wild type) was also apparent when the strains were grown as fumarate fermenters, in the absence of sulfate. Under all of these conditions, the final optical density of the mutant cultures was less than that of the wild type (Figure 2). The mutant strains exhibited diauxic growth under each of these growth conditions whereas the wild type did not (Figure 2).

3.2 Lipid profiles

We quantified the abundance of fatty acid structures in each of the three strains under all five experimental conditions (i.e. pyruvate/sulfate, malate/sulfate, fumarate/sulfate, fumarate fermentation, or pyruvate fermentation). Fatty acids ranged in carbon number from 14 to 18, and both saturated and monounsaturated fatty acids were present. Branched-chain fatty acids of the iso and anteiso series are present in all three strains under all five experimental conditions. Branched fatty acids contained a total of 15 to 18 carbons.

Differences in the lipid profiles of the mutant relative to the wild type were apparent only under the three conditions in which the mutant showed a growth defect: malate/sulfate, fumarate/sulfate, and fumarate fermentation (Figures 3B, 3C, 3D). During growth on malate/sulfate, the *nfn*AB-2 mutant strains contain a higher proportion of anteiso-C17:0, and a lower proportion of C16:0, C18:0, and iso-C15:0 fatty acids. A similar pattern is seen in the mutants during growth on fumarate/sulfate and during fumarate fermentation, although the C18 patterns are slightly different. Differences in anteiso-C17:0 fatty acid is most pronounced in these three growth conditions. In contrast, during both respiratory and fermentative growth on pyruvate, the fatty acid profile of the wild type and mutants were nearly identical (Figures 3A, 3E). Across all strains and conditions, there is a weak inverse correlation between the proportion of branched fatty acids and mass weighted fractionation (Figure S1). Data used to generate these plots are deposited in a permanent repository at Figshare: doi:10.6084/m9.figshare.2132731.
[*Please see temporary link below. The above link is inactive until this MS is accepted, and is permanent and non-editable once activated. The following link is active during review and hosts all SOM files:* https://figshare.com/s/08e9f7b9a5e2e592640f].

3.3 Lipid D/H fractionations

We calculated δD_{total} as the weighted average of the δD_{lipid} of each individual fatty acid pool produced in each strain. We then calculated (Sessions and Hayes, 2005) a total apparent fractionation (ε_{total}) for the fatty acid pool. The results are shown in Figure 4. Apparent fractionations produced by the wild type strain were not discernable between pyruvate/sulfate respiration (ε_{total} = -171‰) and pyruvate fermentation (ε_{total} = -168‰). Similarly, both *nfn* mutants have ε_{total} = -171‰ when grown by pyruvate/sulfate

respiration. However, *nfn* mutants that grew by fermenting pyruvate had smaller fractionations (ε_{total} = -160‰ for the *nfnA*-2 mutant and ε_{total} = -162‰ for the *nfnB*-2 mutant).

Differences in ε_{total} were more pronounced in the other growth conditions. In comparison to growth on pyruvate, the wild type strain showed smaller ε_{total} as a consequence of malate/sulfate growth (ε_{total} = -143‰), fumarate/sulfate growth (ε_{total} = -135‰), and fumarate fermentation (ε_{total} = -142‰). The *nfn* mutants showed even stronger isotopic phenotypes. The *nfnA*-2 mutant had smaller ε_{total} than the wild type during growth on malate/sulfate (ε_{total} = -82‰), fumarate/sulfate (ε_{total} = -103‰), and fumarate (ε_{total} = -108‰). The *nfnB*-2 showed consistently smaller fractionations than both the wild type and the *nfnA*-2 mutant on malate/sulfate (ε_{total} = -59‰), fumarate/sulfate (ε_{total} = -72‰), and fumarate (ε_{total} = -72‰).

The δD_{lipid} of individual lipids can help explain some of these patterns. Most lipids from our cultures were depleted in deuterium by between -50‰ and -250‰ relative to the water in the growth medium. Figures 5 and S2 summarize the results from each strain. The various lipid structures produced by each strain had a wide range of ε_{lipid}, but isotopic ordering among lipids was remarkably consistent. Figure 5A shows ε_{lipid} values for the most abundant lipids in each combination of strain and culture conditions. For all three strains, across nearly every culture condition, the fatty acid with the largest ε_{lipid} was C16:0. The only exception to this were the pyruvate fermentation experiments, in which the largest ε_{lipid} observed was in anteiso-C17:1 in all three strains, and in the fumarate fermentation by the mutants, where the C16:0 was too low in abundance to make isotopic measurements (Figure 5A). The lipid with the smallest ε_{lipid} was uniformly iso-C18:0, and was in some cases enriched relative to media water (Figure 5A).

This suggests that the variations in ε_{total} were mainly a function of a systematic change in ε from one condition to another. Changes in the relative proportion of individual lipids that are particularly enriched or depleted in deuterium. Figure 5B shows the deviation of ε_{lipid} for each individual lipid relative to the ε_{total} for that strain and culture condition. With few exceptions, a consistent pattern emerged in the relative fractionation of each lipid relative to the weighted average. Together, Figures 4 and 5 indicate the presence of significant differences between the wildtype and mutants for growth on malate/sulfate, fumarate/sulfate or fumarate fermentation, while little to no difference existed between strains grown on pyruvate/sulfate or pyruvate fermentation.

We examined whether changes in the abundance of particular lipids were correlated with each other, with growth rate, or with ε_{total}. A graphical display of Pearson correlation indices for each variable pair is shown in Figure 6. This indicates that ε_{total} is strongly correlated with the relative abundance anteiso-C17 fatty acid, and negatively correlated with C16 and C16:1 fatty acid. However, the relative abundance of each of these fatty acids was strongly correlated (negatively, for anteiso-C17 fatty acid) with average growth rate (μ). Growth rate emerged as a strong correlate of ε_{total}. This correlation is shown in Figure 7.

4. Discussion

4.1 Hydrogen isotopes and intracellular electron flow

This study aims at improving understanding of the specific cellular mechanisms that contribute to the D/H ratios in lipids. Zhang et al. (2009) suggested that mechanisms related to the purine dinucleotide coenzymes NAD(P)H were likely to be central to determining lipid δD. In particular, that work suggested that H-isotopic fractionation by transhydrogenase was one potential mechanism for changing the H-isotopic composition the transferable hydride on NAD(P)H. NAD(P)H directly provides approximately 50% of lipid hydrogen, and changes in δD of NAD(P) or the ratios of its oxidized to reduced forms in cells could be effective mechanisms for impacting δD_{lipid}.

Previous work on hydrogen isotope fractionation in sulfate reducing bacteria (SRB) includes studies of pure cultures of *Desulfobacterium autotrophicum* (Campbell et al., 2009; Osburn, 2013), *Desulfobacter hydrogenophilus* (Osburn, 2013) and of *Desulfococcus multivorans* in pure culture and in co-culture with a methanogen (Dawson et al., 2015). Results contrast with those obtained from aerobes, in which growth on different carbon sources results in a large range of ε_{total} (Zhang et al., 2009). *D. autotrophicum* shows only a small range in ε_{total} during heterotrophic growth on acetate, succinate, pyruvate, glucose, or formate, or during autotrophic growth on H_2/CO_2, yet there are large differences in the ε_{lipid} of individual fatty acids (Campbell et al., 2009; Osburn, 2013). Similarly *D. hydrogenophilus* and *D. multivorans* grown in pure cultures have only a small range of ε_{total} during heterotrophic growth (Dawson et al., 2015; Osburn, 2013), with a particularly muted range of ε_{total} during growth of *D. multivorans* in co-culture.

In sulfate reducing bacteria, transhydrogenase NfnAB plays an important role in energy metabolism (Pereira et al., 2011; Price et al., 2014). If this transhydrogenase strongly impacts hydrogen isotope fractionation, it might play a large role in the δD observed in lipids, including any variations in δD as a function of substrate. In this model, NAD(P)H is produced or consumed by a variety of metabolic reactions in the cell, but cycling of NAD(P)H through NfnAB could play a dominant role in determining the δD of NAD(P)H. In addition, δD_{lipid} might be closely coupled to the size of the pools of oxidized and reduced purine dinucleotide coenzymes, rather than simply a function of changes in NAD(P)H δD. The perturbation of NfnAB in mutant strains would be expected to affect the relative sizes of these pools, and could help explain the observed patterns in lipids.

If NfnAB is important in determining δD_{lipid} in SRB, it could also be significant in other anaerobes as well. NfnAB genes are widely distributed in anaerobes, particularly in Deltaproteobacteria, Thermotogae, Clostridia, and methanogenic archaea (Buckel and Thauer, 2013), and nearly ubiquitous in sulfate-reducing bacteria (Pereira et al., 2011). Figure 8 shows the relationship of NfnAB sequences from a range of anaerobes. While *nfnAB* sequences tend to cluster phylogenetically, the gene tree shown in Figure 8 identifies potential lateral gene transfer events among the SRB. The NfnAB genes from

Desulfobulbus propionicus and *Syntrophobacter fumaroxidans* are more similar to those of the methanogenic archaea rather than the other SRB in the Deltaproteobacteria (including *D. alaskensis* G20), which cluster together. Similar to *D. alaskensis* G20, *D. propionicus* and *S. fumaroxidans* are SRB that are capable of fermentative growth on compounds such pyruvate (both) and fumarate (*S. fumaroxidans*).

Other electron bifurcating hydrogenases of note include the multisubunit [FeFe]hydrogenase from *Thermotoga maritima* (HydABC) and from acetogenic bacteria, the [NiFe]hydrogenase/heterodisulfide reductase (MvhADG–HdrABC) from methanogenic archaea (Buckel and Thauer, 2013; Wang et al., 2013a, 2013b). Two other families of transhydrogenases are common in aerobes, including the proton-translocating transydrognease PntAB, and the energy-independent transhydrogenase UdhA (Sauer et al., 2004).

In *D. alaskensis* G20, the catalytic role of NfnAB seems to correlate with δD_{lipid}. During growth on pyruvate/sulfate, electrons are predicted to flow from pyruvate to ferredoxin. Price et al. (2014) suggest that the electrons from ferredoxin flow through NfnAB to produce reduced NADPH. That study pointed out that this transhydrogenase reaction is probably required to produce sufficient NADPH for biosynthesis, although the experiments were done in the presence of yeast extract, which minimized the importance of this reaction. In contrast, our isotopic experiments used a defined medium lacking yeast extract, so the importance of this reaction would not be minimized. NfnAB might be essential to producing sufficient NADPH for biosynthetic reactions. For both the wild type and mutant, growth on pyruvate/sulfate produced lipids that uniformly had the largest ε_{total} across all four experiments.

Sulfate reduction using malate results in NfnAB catalyzing an electron bifurcation in which NADPH reduces NAD^+ and ferredoxin (Price et al., 2014). Fumarate respiration operates in a manner similar to malate. These two substrates can be interconverted by fumarase (Price et al., 2014), so this similarity is likely to be related to similar growth and electron flow. Growth on each of these substrates produces similar patterns in hydrogen isotope fractionation. In each case, the wild type strain produces lipids with ε_{total} near -140‰, which is not as depleted in deuterium as lipids produced during growth on pyruvate. In contrast to growth on pyruvate, the mutant strains have substantially smaller ε_{total}. One explanation for this difference is that the mutation of one paralog of NfnAB in this strain changed the ratio of reduced to oxidized dinucleotides in the cell, with a higher ratio of NADPH to $NADP^+$ and a lower ratio of NADH to NAD^+. A second possibility is that the change in ε_{total} is a consequence of the growth defect of the mutant strains.

Previous work has investigated the relationship of growth rate to ε_{total}. Zhang et al. (2009) did not observe a systematic relationship in the aerobic organisms that they studied. However, a negative relationship was observed between growth rate and the water-alkenone hydrogen isotope fractionation in the coccolithophores *Emiliania huxleyi* and *Gephyrocapsa oceanica* (Schouten et al., 2006). This observation is similar to that reported here, although the slope is steeper for *D. alaskensis* G20. Microbial lipids were recently reported to change their δD_{lipid} with growth phase (Heinzelmann et al., 2015),

although this effect was relatively minor. Algal lipids have been reported to modulate δD_{lipid} as a function of physiological state (Romero-Viana et al., 2013). Each of these relationships could be conceivably related to changes in the turnover rate or ratios of intracellular metabolites, but specific metabolomics data elucidating these relationships has yet to be produced.

Fermentation of pyruvate by *D. alaskensis* G20 likely involves the reduction of pyruvate with NADH by malic enzyme (ME; Dde_1253) to malate (Meyer et al., 2014), which is then dehydrated by fumarase to fumarate, and then reduced to succinate. The oxidative part of this fermentation involves the transformation of pyruvate to acetate, which reduces ferredoxin. Reduced ferredoxin is recycled via flavin-based electron bifurcation, catalyzed by Hdr-Flox-1 (Meyer et al., 2014), but may also interact with NfnAB in the same way as during pyruvate respiration, in an electron confurcation reaction involving NADH, producing NADPH. Wild type *D. alaskensis* G20 grown by pyruvate fermentation produced lipids that showed ε_{total} comparable to that produced during pyruvate respiration. However, the *nfn* mutants grown by pyruvate fermentation had smaller ε_{total} than the wild type. If the *nfn* mutation inhibited NADPH formation, this pattern is opposite of that seen in other experiments, because it results in a smaller ε_{total} at a lower predicted NADPH/NADP ratio. However, the magnitude is small and the important electron bifurcations in ferredoxin recycling may be complicating this interpretation. Unlike the result in Meyer et al. (2014), *nfn* mutants in our experiments did not show a growth defect on pyruvate fermentation. This may in part be related to partial pressures of H_2 produced by growing strains (not monitored herein).

Fumarate fermentation in sulfate reducing bacteria is not well studied, but it is likely a complex metabolism. Wild type *D. alaskensis* G20 has nearly identical growth rates during fumarate fermentation and respiration. The *nfn* mutants grow more slowly than the wild type, but show little difference between fumarate fermentation and respiration. Respiration and fermentation of fumarate, along with respiration of malate, show nearly identical patterns in growth rate and in ε_{total} for each of our three strains (Figure 4). This suggests an underlying mechanism uniting these growth conditions

Fatty acid profiles across the three strains and five conditions show some correlations with the isotope total fractionation (Figure 6). The fractional abundance of branched chain lipids, particularly anteiso-C17:0, are positively correlated with the fractionation and negatively correlated with growth rate. Figure 9 shows three ways in which changing δD values of fatty acids could result in a smaller ε_{total}. First, the ε_{lipid} could be invariant for each individual lipid, but lipid abundances could change. Second, there could be a change in the isotopic ordering of lipids, resulting in a net change in ε_{total}. Third, there could be a consistent change in the ε_{lipid} of most or all lipids. Data shown in Figures 3 and 5 rule out the first two options, and show that all ε_{lipid} change consistently between conditions. This suggests that the driving mechanism for changing in ε_{total} relates to process relevant to all lipids. Processes related to the production and consumption of NADPH are consistent with this role.

By integrating data from all five experimental conditions and three strains, a clear pattern emerges, showing growth rate may be critical in determining δD_{lipid} in SRB (Figure 7). We do not yet have a theoretical prediction for the nature of this relationship, however the relationship is consistent with a linear, exponential decay, or hyperbolic relationship between growth rate and isotope fractionation. This pattern is similar, although opposite in sign, to that seen in sulfur isotope fractionation imposed by SRB during dissimilatory sulfate reduction (Leavitt et al., 2013; Sim et al., 2013). Models aimed at addressing the growth rate—fractionation relationship in sulfur isotopes have focused on ratios of intracellular metabolites and redox state (Bradley et al., 2016; Wing and Halevy, 2014). Similar controls could be at work in controlling hydrogen isotope fractionation: ratios of NAD(P)H/NAD(P)$^+$ and intracellular redox state are related and the partitioning of hydrogen between these pools could exert a direct effect on δD_{lipid}. Work to test this hypothesis, through growth of SRB under conditions of constant rate, are ongoing. If this hypothesis holds, then ε_{total} and δD_{lipid} of sulfate reducers may be able to provide a critical constraint on the interpretation of sulfur isotope patterns in natural systems, such as marine sediments and anoxic water columns. Furthermore, because the *nfnAB* genes are widely distributed in anaerobes (Figure 8), the role of electron bifurcating transhydrogenase in influencing sedimentary lipid H-isotopic distributions is potentially significant. The metabolic role of NfnAB has been investigated in other anaerobes (Lo et al., 2015), and studies of hydrogen isotope fractionation using these strains may indicate whether the patterns uncovered here in sulfate reducers are more generally applicable throughout the microbial domains of life.

5. Conclusions

The magnitude of hydrogen isotope fractionation in *D. alaskensis* G20 is influenced by the growth substrate, with growth on pyruvate exhibiting a different isotopic phenotype than growth on other substrates. Wild type and *nfnAB-2* mutants show large differences in ε_{total} under conditions in which NfnAB-2 is predicted to catalyze an electron bifurcation. This phenotype was observed across the entirety of the *D. alaskensis* G20 fatty acid profile. While ε_{total} correlates with modest changes in the fatty acids produced, it cannot be accounted for by changes in the abundance of individual lipids. These changes in apparent fractionation indicate a role for NfnAB-2 in determining the δD_{lipid} for this strain, which could be significant for explaining δD_{lipid} in other anaerobes due to the wide phylogenetic distribution of this enzyme. However, this interpretation is complicated by growth rate differences between the strains. Using the current data, a relationship in which δD_{lipid} is entirely explained by growth rate cannot be excluded. Future work will aim to isolate these variables and further strengthen our understanding for the roles of growth and metabolic rate as well as electron-bifurcation during H-isotopic fractionation in environmentally key anaerobic metabolisms.

6. Acknowledgements

We thank Dr. A. Deutschbauer and Dr. J. Ray (Lawrence Berkeley National Laboratory) for providing *D. alaskensis* G20 mutant and wildtype strains, Dr. M. Osburn (Northwestern University) for water H isotope measurements and discussions of our data, and Dr. M. Lefticariu (Southern Illinois University, Carbondale) for external verification of lab H isotope standards. We also thank undergraduate researchers C. Wallace and L. Johnson (Washington University in St. Louis, WashU) for laboratory assistance. W. Leavitt acknowledges Washington University for the Steve Fossett Postdoctoral Fellowship. T. Flynn acknowledges support from the Subsurface Science Scientific Focus Area at Argonne National Laboratory supported by the Subsurface Biogeochemical Research Program, U.S. Department of Energy (DOE) Office of Science, Office of Biological and Environmental Research, under DOE contract DE-AC02-06CH11357. This work was funded by NASA Exobiology grant 13-EXO13-0082.

7. References

Bizouarn, T., Grimley, R. L., Cotton, N. P. J., Stilwell, S. N., Hutton, M., and Jackson, J. B. (1995). The involvement of NADP(H) binding and release in energy transduction by proton-translocating nicotinamide nucleotide transhydrogenase from Escherichia coli. *BBA - Bioenerg.* 1229, 49–58.

Bradley, A. S., Leavitt, W. D., Schmidt, M., Knoll, A. H., Girguis, P. R., and Johnston, D. T. (2016). Patterns of sulfur isotope fractionation during Microbial Sulfate Reduction. *Geobiology* 14, 91–101.

Buckel, W., and Thauer, R. K. (2013). Energy conservation via electron bifurcating ferredoxin reduction and proton/Na+ translocating ferredoxin oxidation. *Biochim. Biophys. Acta - Bioenerg.* 1827, 94–113.

Campbell, B. J., Li, C., Sessions, A. L., and Valentine, D. L. (2009). Hydrogen isotopic fractionation in lipid biosynthesis by H2-consuming Desulfobacterium autotrophicum. *Geochim. Cosmochim. Acta* 73, 2744–2757.

Dawson, K. S., Osburn, M. R., Sessions, A. L., and Orphan, V. J. (2015). Metabolic associations with archaea drive shifts in hydrogen isotope fractionation in sulfate-reducing bacterial lipids in cocultures and methane seeps. *Geobiology*, n/a–n/a.

Edgar, R. C. (2004). MUSCLE: Multiple sequence alignment with high accuracy and high throughput. *Nucleic Acids Res.* 32, 1792–1797.

Hayes, J. M. (2001). "Fractionation of the isotopes of carbon and hydrogen in biosynthetic processes," in *Stable Isotope Geochemistry, Reviews in Mineralogy and Geochemistry*, 225–278.

Heinzelmann, S. M., Villanueva, L., Sinke-Schoen, D., Sinninghe Damsté, J. S., Schouten, S., and van der Meer, M. T. J. (2015). Impact of metabolism and growth phase on the hydrogen isotopic composition of microbial fatty acids. *Front. Microbiol.* 6, 1–11.

Jackson, J. B. (2003). Proton translocation by transhydrogenase. *FEBS Lett.* 545, 18–24.

Jackson, J. B., Peake, S. J., and White, S. a. (1999). Structure and mechanism of proton-translocating transhydrogenase. *FEBS Lett.* 464, 1–8.

Kuehl, J. V, Price, M. N., and Ray, J. (2014). Functional Genomics with a Comprehensive Library of Transposon.

Larsson, A. (2014). AliView: A fast and lightweight alignment viewer and editor for large datasets. *Bioinformatics* 30, 3276–3278.

Leavitt, W. D., Halevy, I., Bradley, A. S., and Johnston, D. T. (2013). Influence of sulfate reduction rates on the Phanerozoic sulfur isotope record. *Proc. Natl. Acad. Sci. U. S. A.* 110, 11244–9.

Letunic, I., and Bork, P. (2011). Interactive Tree of Life v2: Online annotation and display of phylogenetic trees made easy. *Nucleic Acids Res.* 39, 475–478.

Lo, J., Zheng, T., Olson, D. G., Ruppertsberger, N., Tripathi, S. a., Guss, A. M., et al. (2015). Deletion of *nfnAB* in *Thermoanaerobacterium saccharolyticum* and its effect on metabolism. *J. Bacteriol.* 197, JB.00347–15.

Marti-Renom, M. A., Stuart, A. C., Fiser, A., Sánchez, R., Melo, F., and Sali, A. (2000). Comparative protein structure modeling of genes and genomes. *Annu Rev Biophys Biomol Struct* 29, 291–325.

Meyer, B., Kuehl, J. V., Price, M. N., Ray, J., Deutschbauer, A. M., Arkin, A. P., et al.

(2014). The energy-conserving electron transfer system used by Desulfovibrio alaskensis strain G20 during pyruvate fermentation involves reduction of endogenously formed fumarate and cytoplasmic and membrane-bound complexes, Hdr-Flox and Rnf. *Environ. Microbiol.* 16, 3463–3486.

Osburn, M. R. (2013). Isotopic proxies for microbial and environmental change: insights from hydrogen isotopes and the Ediacaran Khufai Formation. PhD Dissertation. California Institute of Technology.

Overbeek, R., Olson, R., Pusch, G. D., Olsen, G. J., Davis, J. J., Disz, T., et al. (2014). The SEED and the Rapid Annotation of microbial genomes using Subsystems Technology (RAST). *Nucleic Acids Res.* 42, 1–9.

Pearson, A. (2014). "Lipidomics for Geochemistry," in *Treatise on Geochemistry: Second Edition*, eds. H. D. Holland and K. K. Turekian (Oxford, United Kingdom: Elsevier), 291–336.

Pereira, I. A. C., Ramos, A. R., Grein, F., Marques, M. C., da Silva, S. M., and Venceslau, S. S. (2011). A comparative genomic analysis of energy metabolism in sulfate reducing bacteria and archaea. *Front. Microbiol.* 2, 69.

Polissar, P. J., and D'Andrea, W. J. (2014). Uncertainty in paleohydrologic reconstructions from molecular δD values. *Geochim. Cosmochim. Acta* 129, 146–156.

Price, M. N., Ray, J., Wetmore, K. M., Kuehl, J. V, Bauer, S., Deutschbauer, A. M., et al. (2014). The genetic basis of energy conservation in the sulfate-reducing bacterium Desulfovibrio alaskensis G20. *Front. Microbiol.* 5, 577.

Qi, H., and Coplen, T. B. (2011). Investigation of preparation techniques for δ2H analysis of keratin materials and a proposed analytical protocol. *Rapid Commun. Mass Spectrom.* 25, 2209–2222. doi:10.1002/rcm.5095.

Rabus, R., Hansen, T. A., and Widdel, F. (2006). *Dissimilatory sulfate- and sulfur-reducing prokaryotes*.

Rabus, R., Venceslau, S. S., Wöhlbrand, L., Voordouw, G., Wall, J. D., and Pereira, I. A. C. (2015). *A Post-Genomic View of the Ecophysiology, Catabolism and Biotechnological Relevance of Sulphate-Reducing Prokaryotes*.

RCoreTeam (2015). R: A language and environment for statistical computing. 3464.

Rodriguez-Ruiz, J., Belarbi, E., S, L. G., and Diego, L. (1998). Rapid simultaneous lipid extraction and transesterification for fatty acid analyses. 12, 689–691.

Romero-Viana, L., Kienel, U., Wilkes, H., and Sachse, D. (2013). Growth-dependent hydrogen isotopic fractionation of algal lipid biomarkers in hypersaline Isabel Lake (Mexico). *Geochim. Cosmochim. Acta* 106, 490–500.

Saito, K., Kawaguchi, A., Okuda, S., Seyama, Y., and Yamakawa, T. (1980). Incorporation of hydrogen atoms from deuterated water and stereospecifically deuterium-labeled nicotinamide nucleotides into fatty acids with the Escherichia coli fatty acid synthetase system. *Biochim. Biophys. Acta* 618, 202–213.

Sauer, P. E., Eglinton, T. I., Hayes, J. M., Schimmelmann, A., and Sessions, A. L. (2001). Compound-specific D/H ratios of lipid biomarkers from sediments as a proxy for environmental and climatic conditions. *Geochim. Cosmochim. Acta* 65, 213–222.

Sauer, U., Canonaco, F., Heri, S., Perrenoud, A., and Fischer, E. (2004). The soluble and membrane-bound transhydrogenases UdhA and PntAB have divergent functions in NADPH metabolism of Escherichia coli. *J. Biol. Chem.* 279, 6613–9.

609 Schouten, S., Ossebaar, J., Schreiber, K., Kienhui, s M. V. M., Langer, G., Benthien, A.,
610 et al. (2006). The effect of temperature, salinity and growth rate on the stable
611 hydrogen isotopic composition of long chain alkenones produced by Emiliania
612 huxleyi and Gephyrocapsa oceanica. *Biogeosciences* 3, 113–119.
613 Sessions, A. L., and Hayes, J. M. (2005). Calculation of hydrogen isotopic fractionations
614 in biogeochemical systems. *Geochim. Cosmochim. Acta* 69, 593–597.
615 Silvestro, D., and Michalak, I. (2012). RaxmlGUI: A graphical front-end for RAxML.
616 *Org. Divers. Evol.* 12, 335–337.
617 Sim, M. S., Wang, D. T., Zane, G. M., Wall, J. D., Bosak, T., and Ono, S. (2013).
618 Fractionation of sulfur isotopes by Desulfovibrio vulgaris mutants lacking
619 hydrogenases or type I tetraheme cytochrome c 3. *Front. Microbiol.* 4, 171.
620 Stamatakis, A. (2006). RAxML-VI-HPC: Maximum likelihood-based phylogenetic
621 analyses with thousands of taxa and mixed models. *Bioinformatics* 22, 2688–2690.
622 The UniProt Consortium (2014). UniProt: a hub for protein information. *Nucleic Acids*
623 *Res.* 43, D204–12.
624 Venning, J. D., Bizouarn, T., Cotton, N. P. J., Quirk, P. G., and Jackson, J. B. (1998).
625 Stopped-flow kinetics of hydride transfer between nucleotides by recombinant
626 domains of proton-translocating transhydrogenase. *Eur. J. Biochem.* 257, 202–209.
627 Wang, S., Huang, H., Kahnt, J., Mueller, A. P., Köpke, M., and Thauer, R. K. (2013a).
628 NADP-specific electron-bifurcating [FeFe]-hydrogenase in a functional complex
629 with formate dehydrogenase in Clostridium autoethanogenum grown on CO. *J.*
630 *Bacteriol.* 195, 4373–86.
631 Wang, S., Huang, H., Kahnt, J., and Thauer, R. K. (2013b). A reversible electron-
632 bifurcating ferredoxin- and NAD-Dependent [FeFe]-Hydrogenase (HydABC) in
633 Moorella thermoacetica. *J. Bacteriol.* 195, 1267–1275.
634 Wing, B. A., and Halevy, I. (2014). Intracellular metabolite levels shape sulfur isotope
635 fractionation during microbial sulfate respiration. *Proc. Natl. Acad. Sci.* 111, 18116–
636 18125.
637 Zhang, X., Gillespie, A. L., Sessions, A. L., Zhang X, Gillespie AL, and Sessions AL
638 (2009). Large D/H variations in bacterial lipids reflect central metabolic pathways.
639 *Proc. Natl. Acad. Sci. U. S. A.* 106, 12580–6.
640
641

642 **TABLE(s)**
643

Average growth rates		
Treatment	Strain	μ_{avg}.±1σ (per hour)
pyruvate + sulfate	wildtype	0.154 ± 0.029
	nfnA-2	0.172 ± 0.029
	nfnB-2	0.168 ± 0.035
malate + sulfate	wildtype	0.067 ± 0.007
	nfnA-2	0.014 ± 0.006
	nfnB-2	0.015 ± 0.004
fumarate + sulfate	wildtype	0.085 ± 0.012
	nfnA-2	0.011 ± 0.002
	nfnB-2	0.007 ± 0.006
fumarate fermetation	wildtype	0.057 ± 0.007
	nfnA-2	0.010 ± 0.002
	nfnB-2	0.015 ± 0.004
pyruvate fermetation	wildtype	0.131 ± 0.007
	nfnA-2	0.120 ± 0.001
	nfnB-2	0.149 ± 0.012

644
645 **Table 1:** Growth rates of *D. alaskensis* G20 wild type and *nfnAB-2* transhydrogenase
646 mutants on different substrates during sulfate respiration or substrate fermentation.
647 Rates were calculated as described in the methods with associated errors. The range in
648 rate is larger for experiments that exhibited bi-phasic (diauxic) growth patters (e.g.
649 fumarate + sulfate), as is apparent from the growth curves (Fig. 2).
650
651

FIGUREs

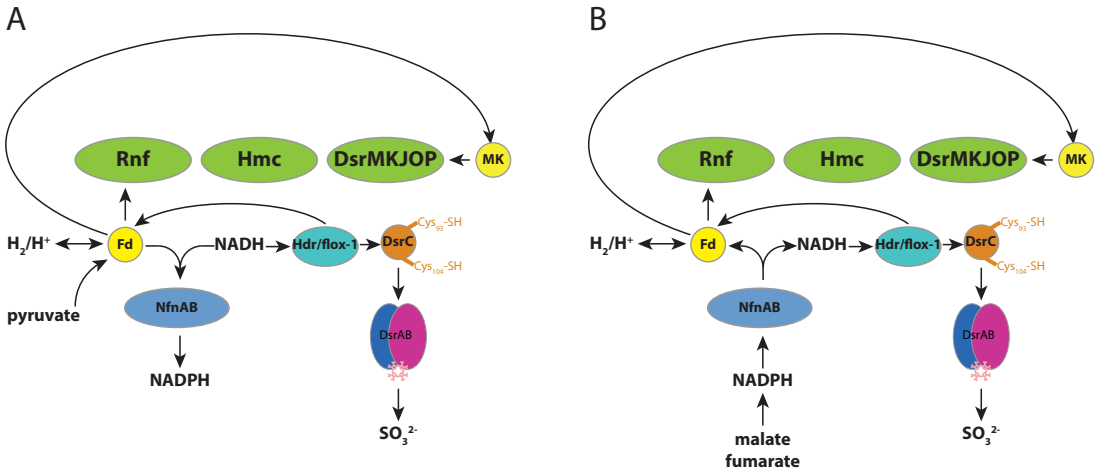

Figure 1. (A). A schematic pathway of electron flow during pyruvate respiration or fermentation in WT *D. alaskensis* G20. Electrons are transferred from pyruvate through ferredoxin and NADPH, and NfnAB catalyzes electron confurcation, producing NADPH. Mutation of NfnAB is predicted to result in deficiency of NADPH (B). Electron flow during fumarate and malate respiration or fumarate fermentation. NfnAB catalyzes electron bifurcation, such that the mutant strains are predicted to have excess NADPH.

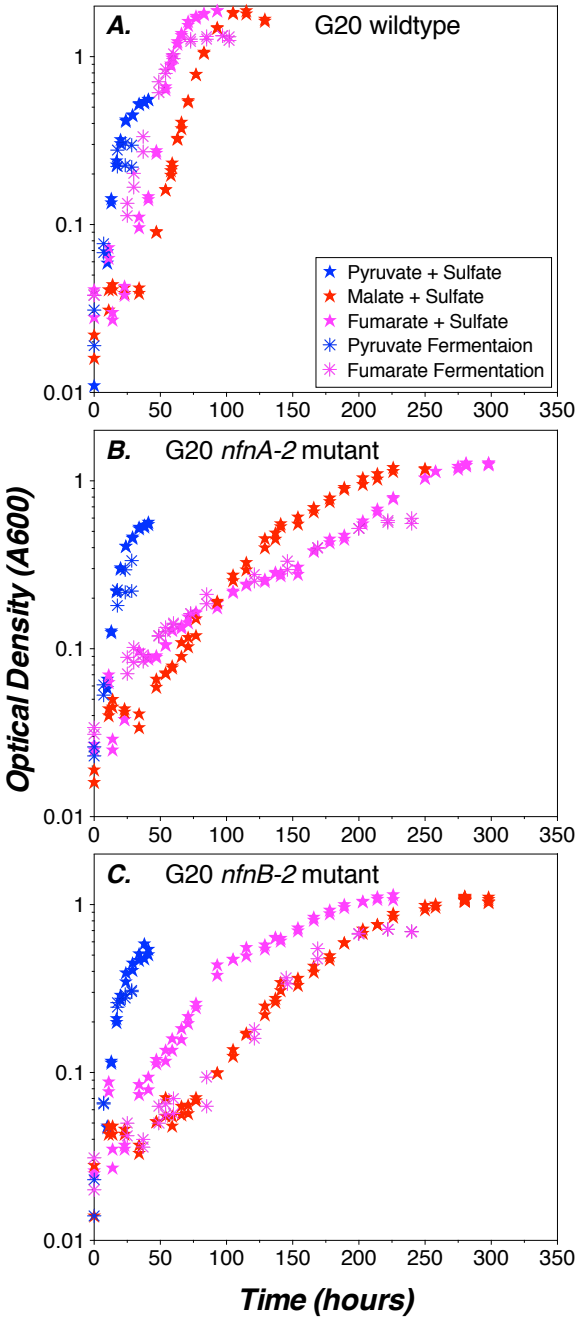

Figure 2. Growth curves for *D. alaskensis* G20 wildtype and transhydrogenase mutants. (A) Wildtype, (B) *nfnA-2* transposon mutant, and (C) nfnB-2 transposon mutant, each under all 5-condition sets tested (denoted in the legends). Each symbol represents the average of biological duplicate 50mL cultures. Error bars are smaller than the symbols in all cases. Samples for lipid and isotopic analysis were extracted after the final time-point indicated on this plot, all in early stationary phase.

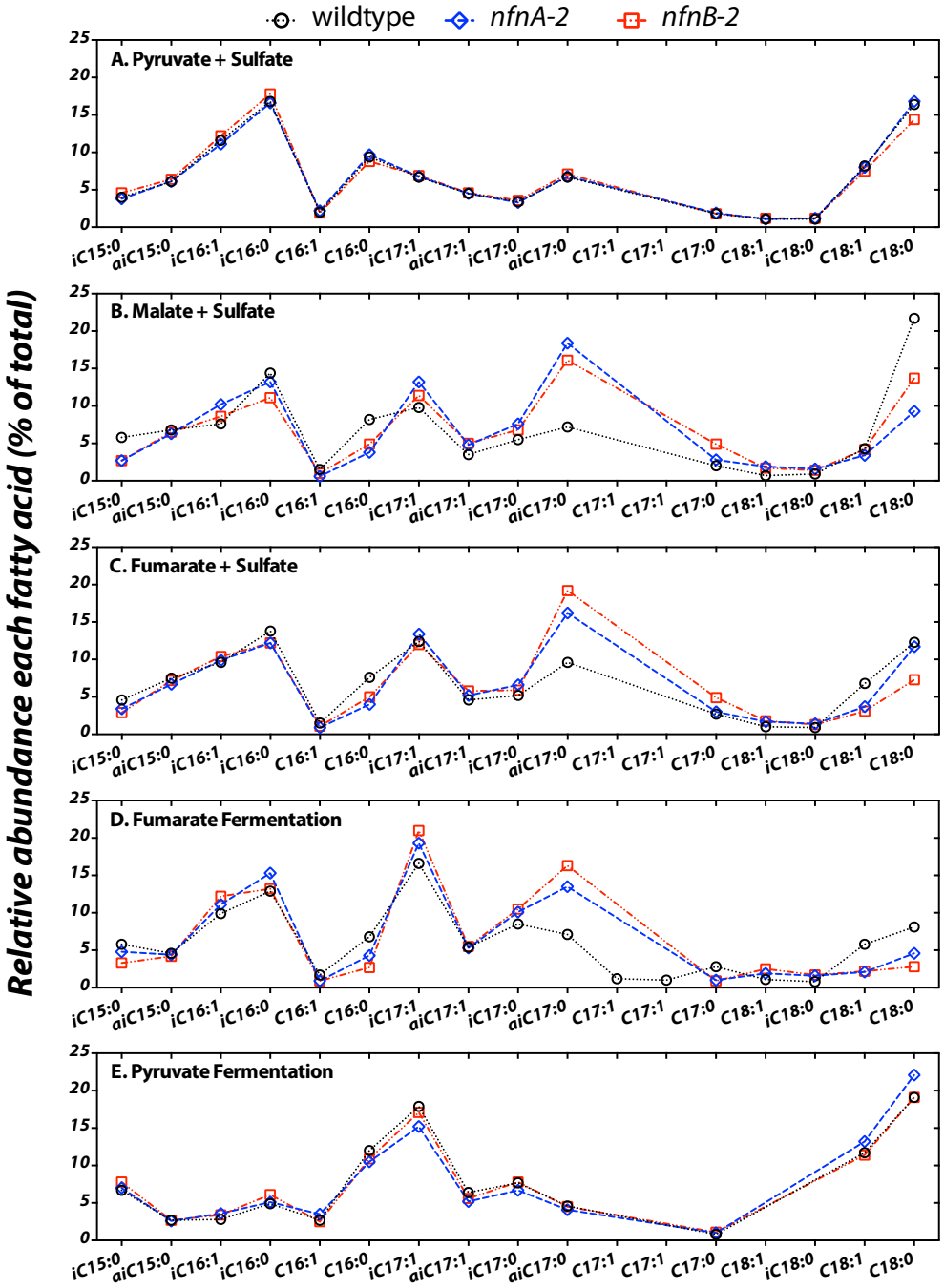

672
673 **Figure 3.** The relative abundance of each fatty acid (% of total) from each strain under
674 the five different growth condition tested (A to E). Sample key: wild type (black circles,
675 dotted lines) or *nfnAB-2* transhydrogenase insertion-deletion mutants, *nfnA-2* (blue
676 diamonds, dashed lines) and *nfnB-2* (red squares, dash-dotted lines). Each symbol is
677 the average of biological replicates for each strain given that condition set, and the
678 standard error of individual fatty acid quantifications is <0.5% between biological
679 replicates (error bar significantly smaller than the symbols).
680

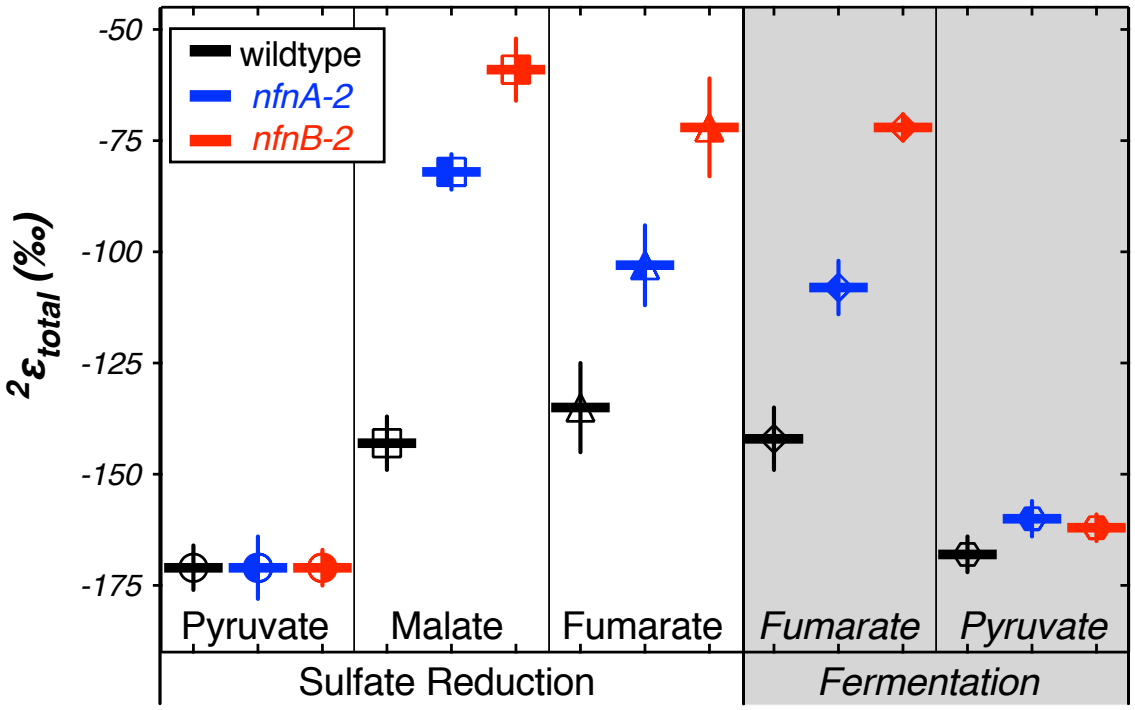

Figure 4. Hydrogen isotope fractionation between media water and the mass-weighted lipid pool for each treatment. The values plotted are the average of biological replicates and weighted average of all individually measured compounds. Vertical bars are standard errors on the mean (SEM).

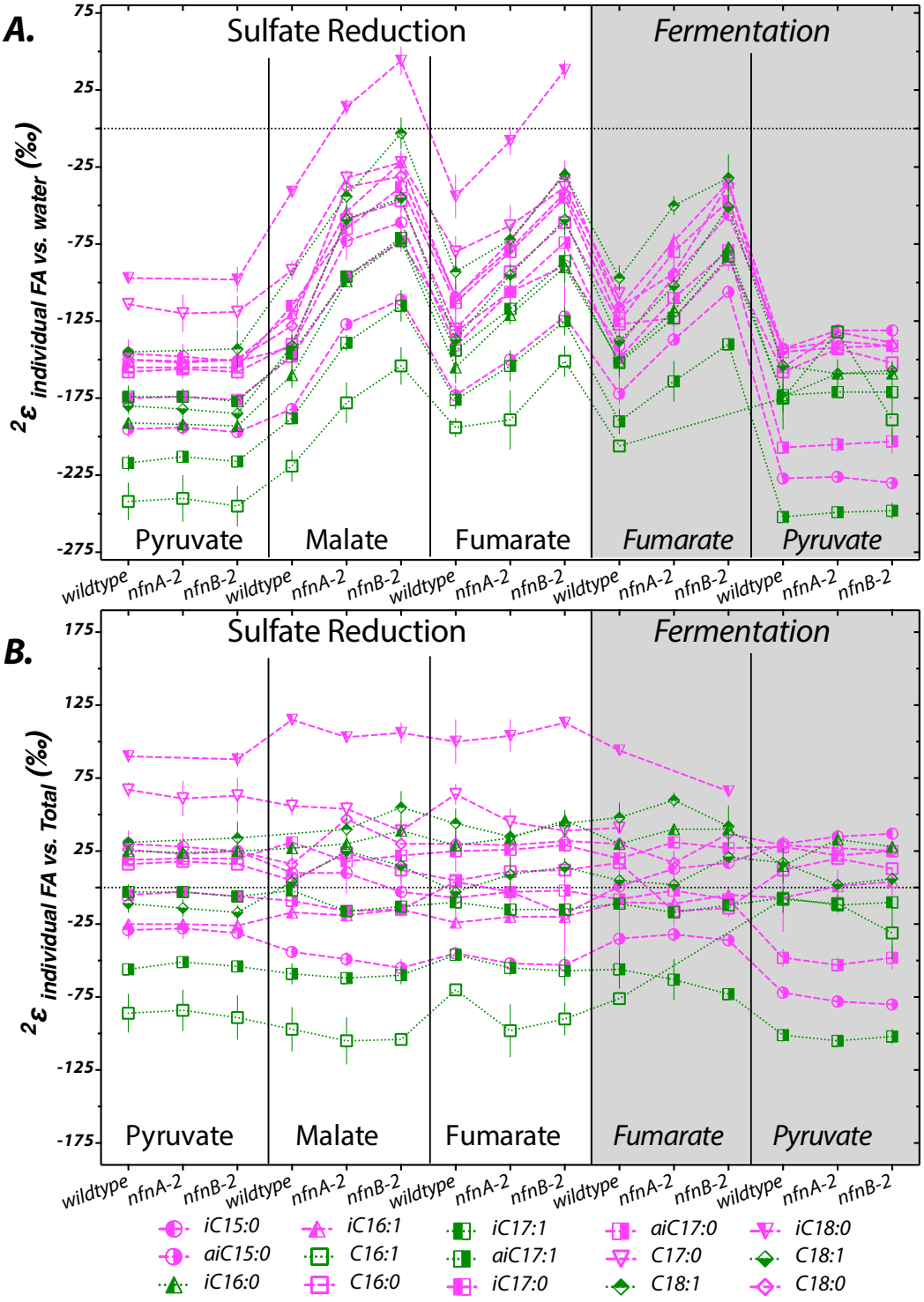

Figure 5. (A) Hydrogen isotope values for individual fatty acids relative to the medium water. (B) Deviation of individual fatty acid H-isotopic composition relative to the weighted mean of each individual experiment. Each symbol represents the mean of biological replicates (N = 2, and technical replication $n_{avg.}$ = 3, range 1 to 6), with SEM.

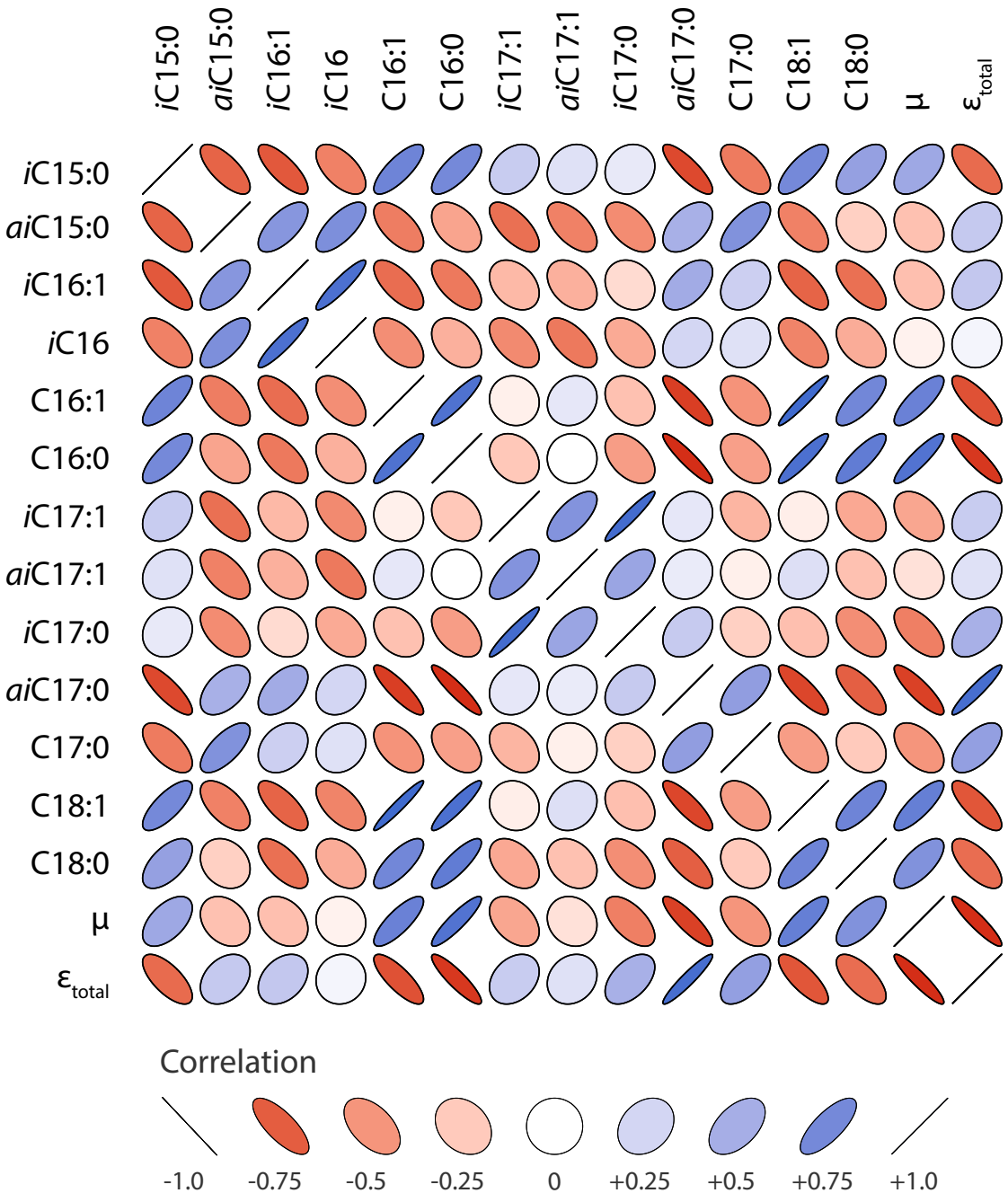

Figure 6. Representation of Pearson correlation indices for each pair of variables. Width of ellipses indicates the strength of the correlation, with narrow ellipses indicating a strong correlation and circles indicating no correlation. Darker blues are stronger positive correlations, darker reds are stronger negative correlations, with white indicating no correlation.

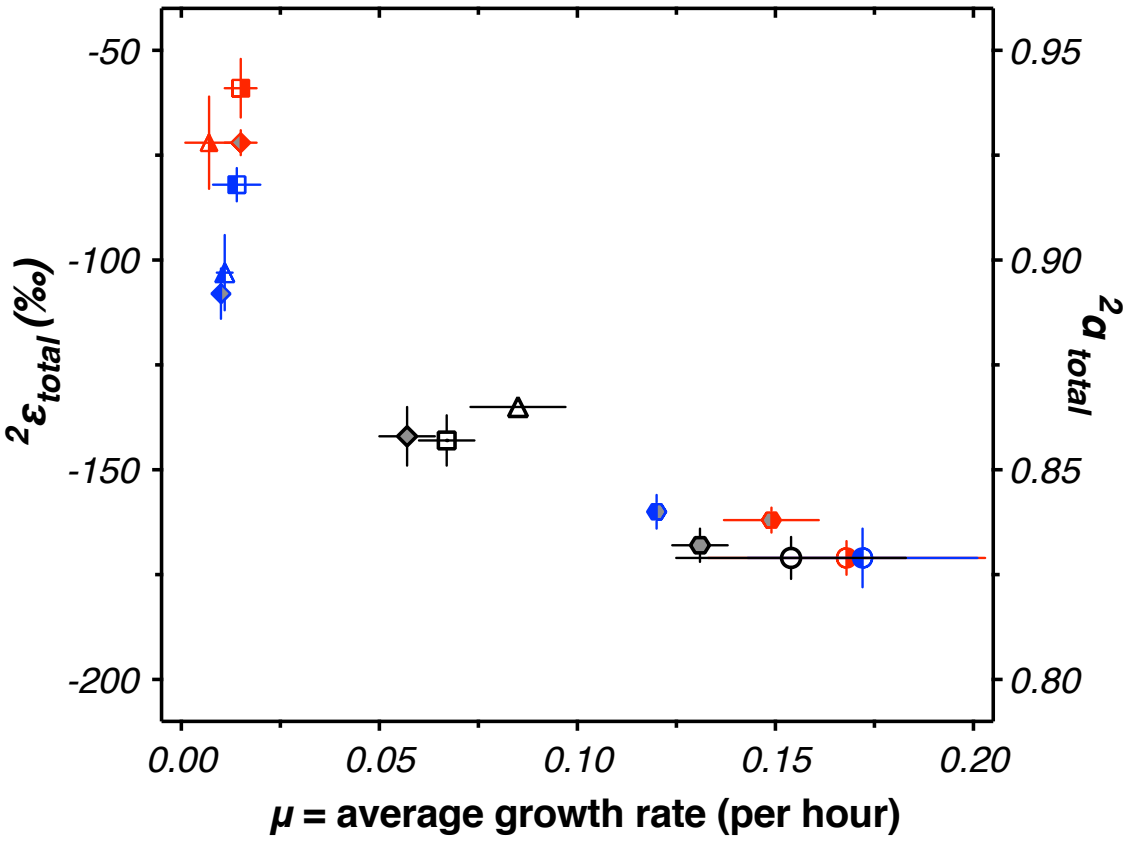

Figure 7. Mean growth rate versus the mass weighted mean H isotope fractionation for all experiments (the values from Table 1 and Figure 4, respectively).

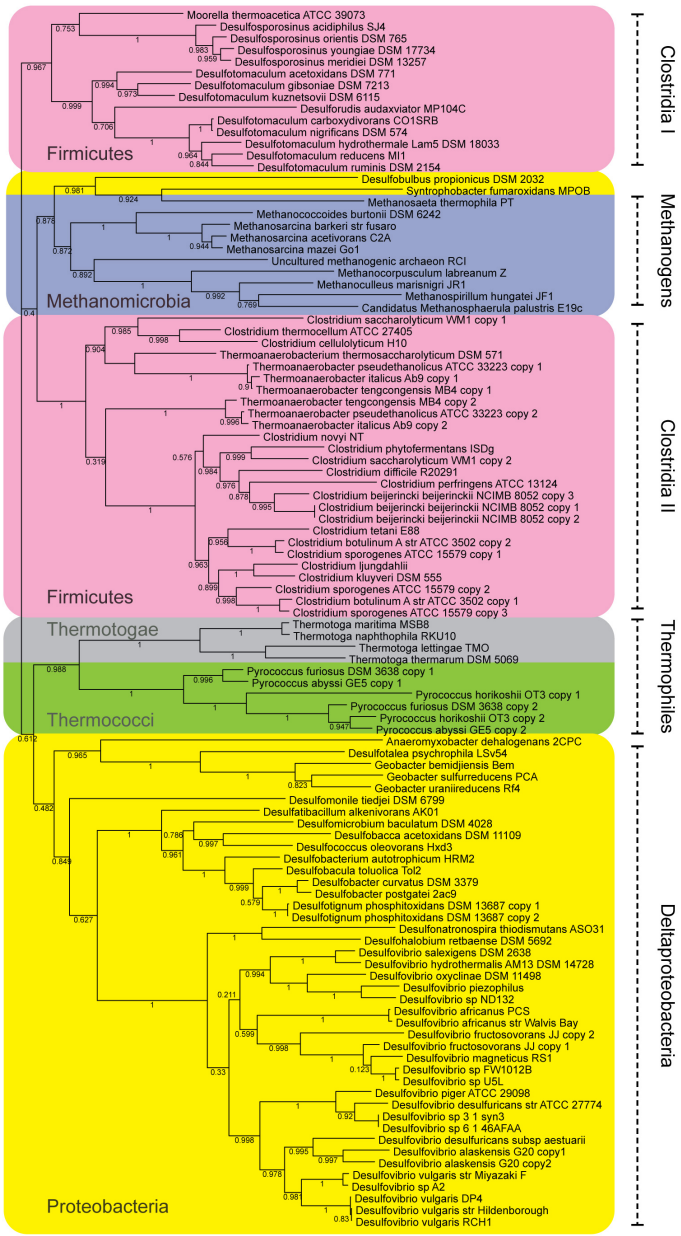

Figure 8. Maximum likelihood phylogenetic tree of NfnAB using amino acid sequences taken from the sequenced genomes of known anaerobes. Each branch is colored by Phylum. Bootstrap values (out of 100) are shown at each branch point.

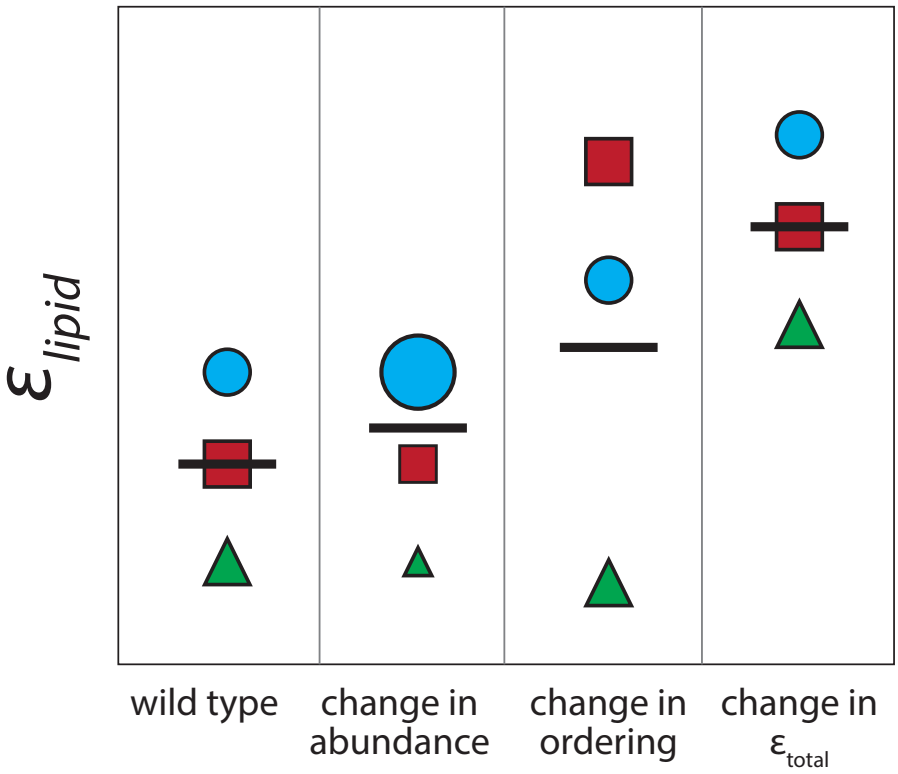

Figure 9. Potential mechanisms for changing the weighted average of D/H in the lipid pool. Colored symbols represent individual lipids, horizontal bar represents weighted average (ε_{total}). Change in abundance: increased abundance of lipids with various ε_{lipid}. Change in ordering: changes in ε_{lipid} that differed among lipids. Change in ε_{total}: a uniform change to the ε_{lipid} of every lipid.

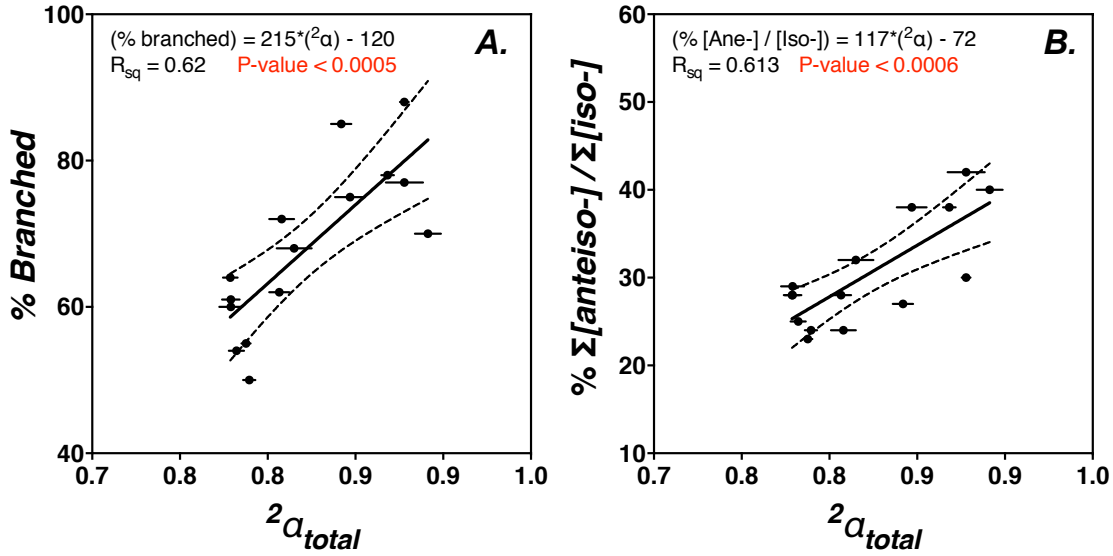

Figure S1. The (A) abundance of branched fatty acids or (B) proportion of anteiso-/iso-branched fatty acids, each relative to ε_{total} for all the conditions tested. The linear regression (solid line) for each is significant (P-value < 0.005), with the 95% confidence intervals plotted as dashed lines.

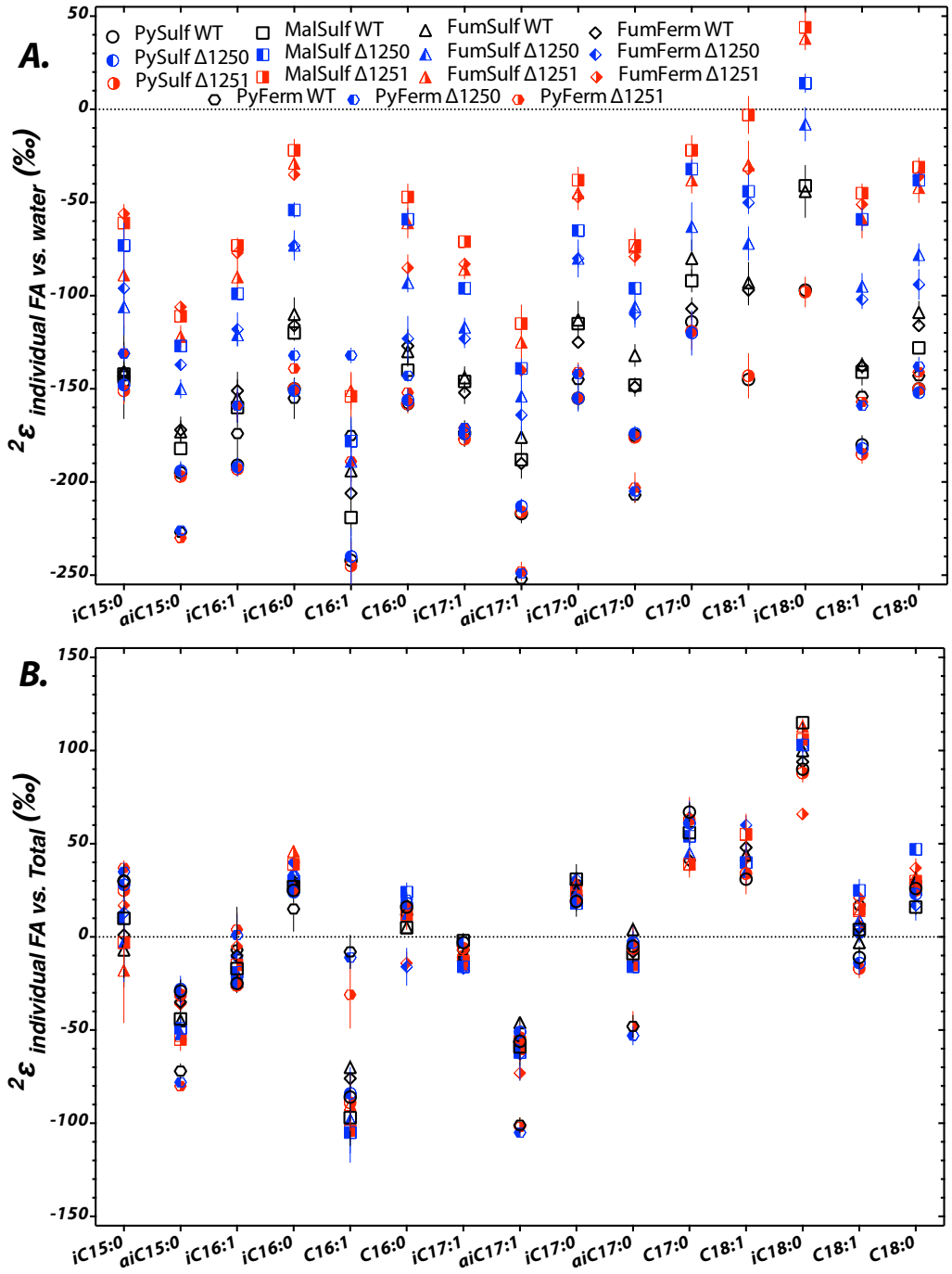

Figure S2. The same values as in Figure 5, here plotted by fatty acid ID (on the X-axis), and coded by experimental combination (see legend).